



Original Paper

Influence of Geological and Environmental Factors on the Reconsolidation Behavior of Fine Granular Salt

Yanfei Kang,^{1,2} Jinyang Fan,^{1,2,3} Deyi Jiang,^{1,2} and Zongze Li^{1,2}

Received 27 April 2020; accepted 11 August 2020

Published online: 18 August 2020

Understanding the consolidation behavior of granular salt is of great significance for salt cavern repository design and the corresponding long-term safety assessments. To evaluate the influence of environmental and geological factors on the reconsolidation behavior of fine granular salt, a series of orthogonal array design experiments were performed. The experimental results showed that temperature, compressive stress, moisture content and compression time had significant impacts on the compaction properties of granular salt. The compressive stress exerted the greatest impact on porosity of the granular salt, which decreased the porosity. An increase in moisture content (within 3%) in the granular salt sample substantially reduced the porosity of the sample, whereas this effect was limited when moisture exceeded 3%. In the process of granular salt compaction, all of the deformation mechanisms were temperature dependent. The correlation between porosity and permeability of the dried compacted salt samples was independent of the environmental and geological factors during the compaction of the granular salt. The use of granular salt with a smaller particle size in the compacted salt backfill can improve its sealing performance. In the transient loading stage of granular salt compaction, the porosity decreased rapidly under stress to form a denser layer, which was mainly accomplished by particle rearrangement and cataclastic flow. However, in the constant-load creep stage, the additional porosity reduction was dominated by grain boundary processes and crystal plasticity mechanisms, including dislocation creep, pressure-solution creep and recrystallization.

KEY WORDS: Salt cavern, Underground gas storage, Granular salt, Feasibility analysis, Deformation mechanism.

INTRODUCTION

Rock salt exists in vast beds of sedimentary evaporite deposits, which are remnants of dried-up lakes, playas and seas. It is a common industrial raw material and food flavor enhancer, which has been

used for thousands of years. Due to its excellent mechanical properties, such as low porosity (Wang et al. 2020), low permeability (Popp et al. 2012; Wu et al. 2020), high-ductility (Jiang et al. 2016; Fan et al. 2019; Fan et al. 2020a) and self-healing capacity (Chen et al. 2018; Kang et al. 2019), rock salt has long been recognized as a highly suitable medium for geological storage/sequestration.

In the past few decades, salt caverns have been proposed as underground storage facilities for oil (Costa et al. 2015; Liu et al. 2019a), natural gas (Schiebahn et al. 2015; Peng et al. 2020; Chen et al. 2020), hazardous wastes (e.g., nuclear wastes, alkali

¹State Key Laboratory of Coal Mine Disaster Dynamics and Control, Chongqing University, Chongqing 400044, China.

²School of Resources and Safety Engineering, Chongqing University, Chongqing 400044, China.

³To whom correspondence should be addressed; e-mail: jy-fan@cqu.edu.cn

residue (Hansen and Leigh 2011), compressed air (Chen et al. 2017; Fan et al. 2018), hydrogen gas (Liu et al. 2016; Tarkowski and Czapowski 2018; Fan et al. 2020b) and flow battery electrolyte (Letcher 2019). To date, more than 40 countries around the world have operated salt caverns for commercial or strategic reserves. The U.S. Strategic Petroleum Reserve currently operates and maintains 60 large underground salt caverns in the Gulf Coast, constituting four major oil storage facilities (Hart 2018). In Germany, nearly half of the natural gas storage facilities are built in underground salt caverns, which have a total working capacity exceeding 14 billion m^3 (Cretì 2009). China is the largest salt producer in the world, with annual output of nearly 50 million tons in recent years. To date, tens of thousands of abandoned salt caverns have been formed underground, and the volume of underground salt caverns is currently increasing by 20 million m^3 per year (Liu et al. 2019a, b, c). In recent years, China has increasingly regarded salt caverns as a strategic resource (Liu et al. 2019b, 2020; Zhang et al. 2020; Li et al. 2020; Qiao et al. 2020). Consequently, China has supported a national key project for the comprehensive application of abandoned salt caverns.

In the utilization of salt caverns, sealing cavity shafts and ensuring tightness is a concerning issue (Khamrat and Fuenkajorn 2018). In China, hundreds of abandoned salt caverns that do not meet the requirements for oil storage and natural gas storage have been proposed as storage facilities for low-hazardous waste (e.g., alkali slag, oilfield sludge, calcium magnesium waste). The shafts of these salt caverns require safe and reliable long-term/permanent closure (Shi et al. 2015). Under such high-salt and highly corrosive conditions, the common sealing materials, such as ordinary concrete, will gradually disintegrate and lose their isolation functionality over time, resulting in hazardous waste leakage and potential groundwater pollution.

Due to the excellent properties of rock salt, granular salt (also known as crushed salt) has been recognized as the most suitable material for sealing salt cavern shafts (Fig. 1a) based on the following points. (a) Granular salt can be compacted, after which its porosity (ϕ) and permeability (K) will decrease. Over long periods of time, granular salt is expected to reconsolidate gradually into a material that is comparable to intact rock salt (Salzer et al.

2007). (b) Artificially compacted granular salt has obvious compatibility with original rock salt, and these materials are expected, because of the self-healing capacity of salt, to be closely integrated. In addition, crushed salt is considered the most promising backfill material for the rooms, drifts or shafts of nuclear waste repositories in salt caverns (Fig. 1b) based on the two above-mentioned points and additional advantages, such as excellent thermal conductivity and low cost. For repository design and long-term safety assessment, understanding the consolidation behavior of crushed salt is of great significance.

In view of the application prospects of compacted granular salt as a sealing and back-filling material for salt cavern reservoirs, many scholars and institutions have shown great interest in the consolidation behavior of granular salt as well as in the performance of compacted salt. In previous studies, the mechanical (Ding et al. 2016; Khamrat et al. 2018), thermal (Bauer and Urquhart 2016; Paneru et al. 2018) and transport performance (Dewers et al. 2015) of compacted salt have been reported to evaluate the feasibility of using compacted granular salt as back-filling and sealing materials. In addition, the stress state (Broome et al. 2014), moisture (Mills et al. 2018), temperature (Olivella et al. 2011; Hansen et al. 2012), pore pressure (Lampe et al. 2018) and other factors that influence the reconsolidation of granular salt have also been a research focus. However, many of these studies focused on only one of these factors and did not consider how this factor influenced the compaction of granular salt, which may result in biased assessment for sealing functionality and long-term repository performance.

In this paper, the effects of temperature, compressive stress, moisture content and compression time on the performance of granular salt reconsolidation were investigated through a group of orthogonal tests. After compaction, the gas K of all the compacted salt samples was measured to reveal the permeation properties of compacted salt. Experiments were carried out over a range of pressures and temperatures that may exist in underground waste repository. Hence, the results of this study can be used as a reference for repository design and safety assessment.

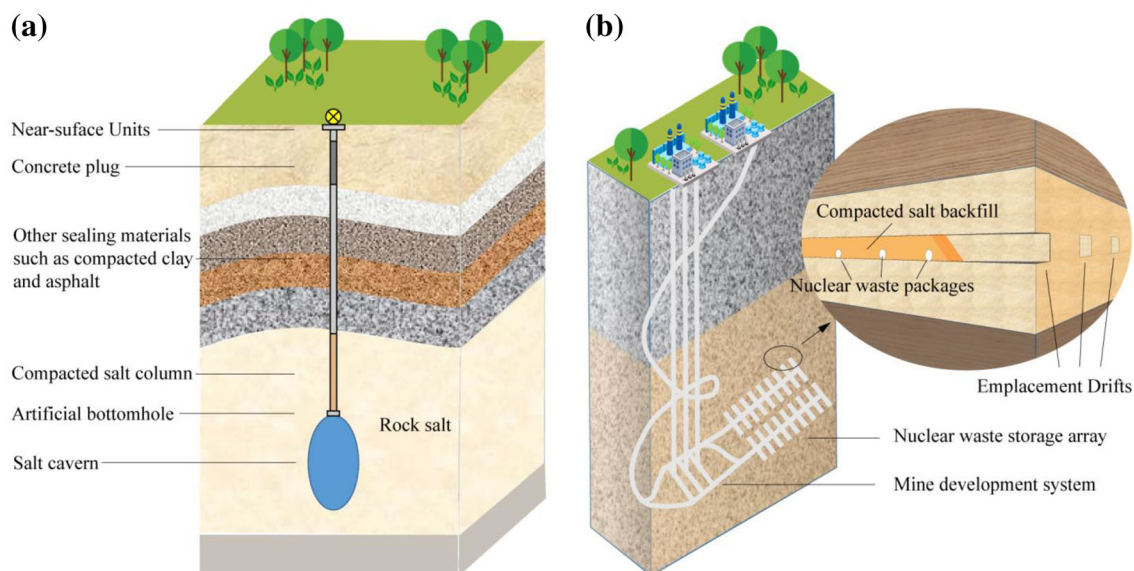


Fig. 1. Schematic diagram of the application of compacted granular salt (a) as sealing material for salt cavern shafts and (b) as backfill material for an underground salt repository of nuclear waste.

MATERIALS AND METHODS

Preparation of Granular Salt

Experimental samples consisted of “mine-run” rock salt excavated from the Khewra salt mines, Pakistan. There are seven salt seams with cumulative thickness of ~ 150 m in the Khewra salt mines, which cover an area of ~ 110 km², as an irregular dome-like structure in pre-Cambrian rocks. The rock salt from these mines is translucent and appears white, pink, reddish or beef-color red. Moreover, this rock salt contains a sodium chloride content greater than 98% and a very small amount of impurities, for which the main component is soluble matter such as sodium sulfate and magnesium chloride (Fig. 2a).

The rock salt used in our experiments was crushed and sieved into granular salt with diameters ranging from 0.25 to 0.42 mm. To limit the influence of the original free water in the material on the experimental results, the granular salt was oven-dried at 110 °C for over 24 h prior to all experiments. Then, an atomizer was used to adjust the moisture in the dried granular salt to achieve the granular salt with a specific moisture content. The dried granular salt was weighed and placed in a large glass dish, and then, the water was turned into a mist through an atomizer and sprayed on the dried salt

powder. All of these operations were performed on a high-precision electronic balance (accuracy 0.01 g) to ensure desired quantity of water was added to the granular salt (Fig. 2b). The salt powder was sprayed with mist many times, and a glass rod was used to mix the powder evenly in each interval. These operations were repeated until the amount of water added to the powder reached a predetermined value. According to our on-site observations (e.g., color, adhesion), this approach can ensure the uniformity of the moisture in the granular salt. Granular salt was obtained with moisture contents of 3, 6, 9 and 12% (Fig. 2c). As the moisture content increased, the degree of adhesion of the granular salt gradually increased.

Backfill Compaction Cell Design

A specially designed backfill compaction cell was used to perform compaction tests without lateral deformation on the granular salt, which simulated odometer-like conditions on cores from boreholes. Figure 3a presents a schematic of the backfill compaction cell.

A computerized, servohydraulic test frame (MTS Systems Corporation) was used to perform the compaction tests. This test frame can provide a total axial load of 400 kN. A linear variable differ-

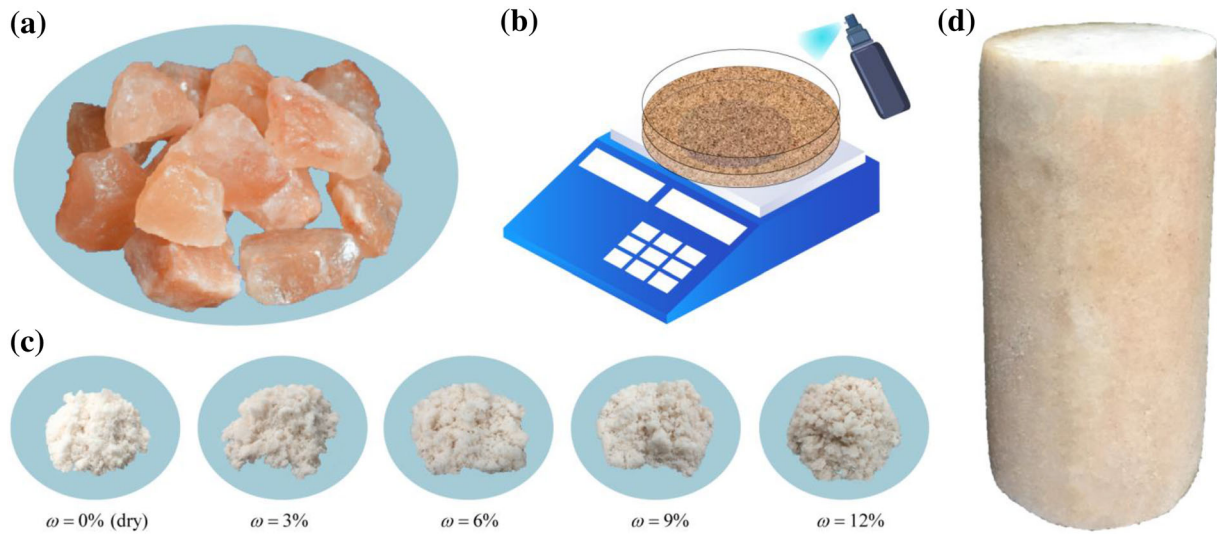


Fig. 2. (a) Rock salt used in our experiment. (b) Using an atomizer to increase moisture in the dried granular salt to achieve a specified moisture content, which was carried out on an electronic balance. (c) Granular salt with moisture contents of 0, 3, 6, 9 and 12%. The degree of adhesion of the granular salt gradually increased as moisture content increased. (d) A sample obtained by compaction of granular salt.

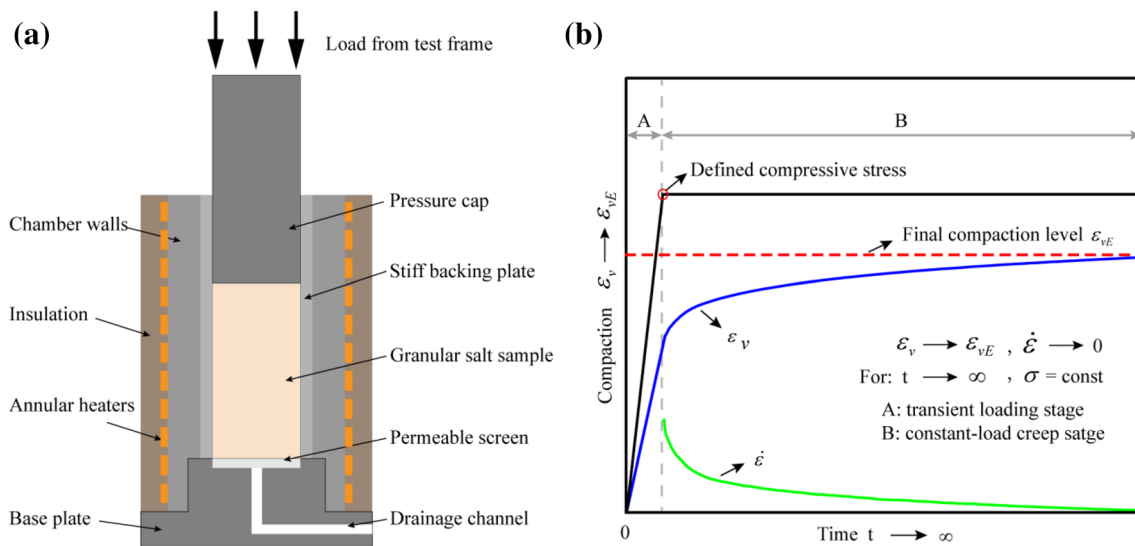


Fig. 3. (a) Schematic of backfill compaction cell. (b) Compaction of granular salt, including schematics of the experimental procedures.

ential transformer (LVDT) mounted outside the compaction cell can monitor the axial displacement (i.e., the compressive deformation of the sample) in real time during the tests. The heating system, which contains a programmable thermostat that regulates power to the annular heaters on the compaction cell, could maintain specimen temperatures of 25–150 °C. Moreover, the thermocouple in the cell wall

supplied the feedback signal. Additionally, the backfill compaction cell adopts three stiff backing plates, which are easy to disassemble during the demolding process after compaction testing. Prior to each test, a thin layer of HR-1200 fluoride release agent was applied to the internal surfaces of the stiff backing plates to reduce the effects of friction during testing.

During the compaction test, the granular salt was compacted in the axial direction by a vertical stress σ_v , which was supplied by the test frame. The salt was also subjected to a horizontal stress σ_h , which was induced by the stiff chamber walls that prevented lateral deformation. According to a previous study by Bechthold et al. (2004), the stress ratio $\lambda = \sigma_h/\sigma_v$ corresponding to compaction with lateral restraint usually ranges between 0.30 and 0.55 and increases as the ϕ of granular salt samples decreases.

Compaction Test Procedure

The compaction test procedure is shown in Figure 3b. First, a predetermined axial pressure was applied to the granular salt sample at a constant loading rate of 0.5 kN/s. Then, the axial pressure was maintained at a constant level to simulate time-dependent compaction processes, i.e., volumetric creep after preloading. The tests conducted in this paper can be separated into the following two stages: (1) the transient loading stage, which is the portion of the test before reaching the preset compressive stress, and (2) the constant-load creep stage, which is the portion of the test after reaching the preset compressive stress. Moreover, it should be noted that the effect of slight changes in lateral stress was ignored in our experiments.

Orthogonal Array Design

Orthogonal array design (OAD) is an important branch of statistical mathematics, which is based on probability theory and mathematical statistics, and is used to design test plans in the form of a standardized orthogonal table. According to Galois theory, OAD is a scientific test design method, which selects the right amount of representative points or uses cases from a large number of experimental data, to arrange experiments or tests reasonably. It is possible to use the corresponding range analysis and the variance analysis to analyze the test results, which are highly reliable and can lead to many valuable conclusions.

A standardized orthogonal table is a two-dimensional digital table characterized by “neat comparability” and “uniform dispersion.” The term “neat comparability” means that when each factor is tested at each level, the other factors are kept the

same, which minimizes the interference of these other factors on the response. Moreover, the factors in the table are uniformly dispersed, which ensures that a complete combination of factors is tested.

In the OAD, the selection of factors is based on previous knowledge of compaction of granular salt. Based on experimental conditions reported by other researchers for the compaction of similar rock particles, the factors that can substantially affect the compaction behaviors of granular salt were identified as temperature, compressive stress, moisture content and compression time. Based on the test conditions available in our laboratory, five levels were determined for each factor (Table 1). Under these conditions, only the $L_{25}(5^6)$ standardized orthogonal table (Table 2), which has six factors and five levels, is appropriate. For our experiments, the four factors indicated above filled only the first four columns of the orthogonal table. Therefore, two null columns were included in the selected $L_{25}(5^6)$ table. According to the theory of OAD, the two null columns can be used to estimate errors caused by other random factors that were not taken into account in the experiments, thereby illustrating experimental reliability. Hence, the last two columns were defined as Error column 1 and Error column 2 (i.e., factors E1 and E2), which were used in the variance analysis to estimate errors caused by random factors; note that, E1 and E2 are completely equivalent. In addition, the values (1–5) in the columns in Table 2 correspond to the experimental levels listed in Table 1.

RESULTS AND ANALYSIS

Overview of Experimental Data

The ϕ of the samples (Fig. 2d) was measured after the experiments. These measurements were

Table 1. Experimental factors and their values at different experimental levels

Factors	Experimental levels				
	1	2	3	4	5
Temperature (°C)	30	45	60	75	90
Compressive stress (MPa)	15	30	45	60	75
Moisture content (%)	0	3	6	9	12
Compression time (min)	50	100	200	400	800

Table 2. $L_{25} (5^6)$ orthogonal array

Exp. no.	*Factors and their levels					
	A	B	C	D	E1	E2
1	1	1	1	1	1	1
2	1	2	2	2	2	2
3	1	3	3	3	3	3
4	1	4	4	4	4	4
5	1	5	5	5	5	5
6	2	1	2	3	4	5
7	2	2	3	4	5	1
8	2	3	4	5	1	2
9	2	4	5	1	2	3
10	2	5	1	2	3	4
11	3	1	3	5	2	4
12	3	2	4	1	3	5
13	3	3	5	2	4	1
14	3	4	1	3	5	2
15	3	5	2	4	1	3
16	4	1	4	2	5	3
17	4	2	5	3	1	4
18	4	3	1	4	2	5
19	4	4	2	5	3	1
20	4	5	3	1	4	2
21	5	1	5	4	3	2
22	5	2	1	5	4	3
23	5	3	2	1	5	4
24	5	4	3	2	1	5
25	5	5	4	3	2	1

*For our experiments, the first four columns (i.e., factor A, B, C and D) correspond to the four factors in Table 1 and the last two columns (i.e., factor E1 and E2) are null columns that serve as error columns. The values/levels (1–5) correspond to the experimental levels listed in Table 1

based on the measured masses and volumes of the samples (referred to as the MV method) and a measured grain density of 2.16 g/cm^2 , which was calculated using Eq. (1). Paneru et al. (2018) presented the MV method in detail and compared the ϕ of consolidated granular salt samples obtained from a porosimeter and the MV method. Their results (Fig. 4) showed that these two methods produced very similar results, which verified that ϕ measured by the MV method is credible.

$$\phi_f = 1 - \frac{\rho_d}{\rho_g} \quad (1)$$

where ρ_d is dry bulk density (g/cm^3) and ρ_g is salt grain density (g/cm^3).

During the compaction tests, deformation of the experimental samples was quantified in terms of the volumetric strain (ε_v), which is considered positive in compression. The ε_v can be calculated under the given conditions (i.e., compaction without lateral

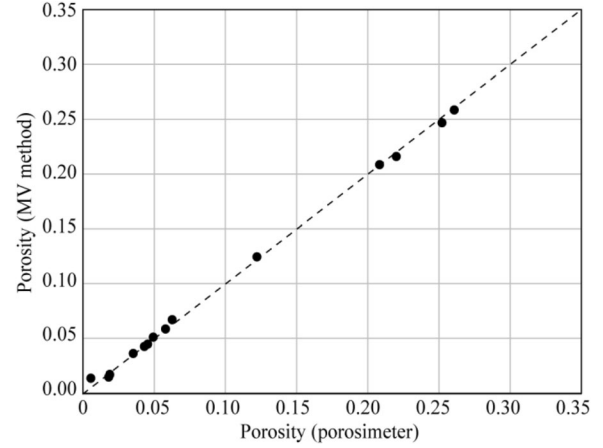


Fig. 4. Comparison of porosities obtained from a porosimeter method and the MV method (Paneru et al. 2018).

deformation) with Eq. 2. In addition, the ϕ during the test can be calculated by vertical deformation of a specimen with (Eq. 3), which is based on the assumption of a constant volume of salt grains. In this case, ϕ and ε_v during the test were dependent and can be converted with Eq. 4.

$$\varepsilon_v = -\frac{V - V_0}{V_0} = 1 - \frac{l}{l_0} \quad (2)$$

$$\phi = 1 - \frac{m}{\rho_g \cdot A \cdot l} \quad (3)$$

$$\phi = 1 - \frac{m}{\rho_g \cdot A \cdot l_0(1 - \varepsilon_v)} \quad (4)$$

where V and l represent the deformed volume and length of a salt sample, respectively, V_0 and l_0 represent the initial volume and initial length of a salt sample, respectively, m is the mass of dry compacted salt specimen, and A is cross-sectional area of a specimen. Because granular salt is loose and contains many pores before loading, the initial length of a salt sample when the axial stress reaches 10 MPa is designated as l_0 of a salt sample to reduce the discreteness of the deformation measurement. The l of a deformed salt sample during the compaction tests can be obtained from the axial displacement monitoring system (i.e., the LVDT). In this paper, the sample deformation during compaction was analyzed in terms of ϕ , ε_v and volumetric strain rate ($\dot{\varepsilon}_v$).

Experimental Loading and Deformation

Twenty-five granular salt samples with different initial moisture contents were subjected to compaction experiments with different temperatures, stresses and compression time according to the orthogonal array shown in Table 2. Due to their similar deformation characteristics, only part of the experiments was selected and presented in this paper (Fig. 5). Representative deformation curves from the transient loading stage of the granular salt samples are shown in Figure 5a, in which the measured axial stress, ε_v , ϕ , and $\dot{\varepsilon}_v$ of sample 75_05 are plotted against the testing time. In the transient loading stage, the ε_v increased and the ϕ decreased as the increasing axial pressure increased.

The measured axial stress, ε_v , ϕ and $\dot{\varepsilon}_v$ against testing time in the creep stage of the selected samples 30_05, 45_04, 60_03, 75_02 and 90_01 is shown in Figure 5b–f. The compression time of these samples in the creep stage was 800 min. The deformation trends of all the samples were similar. Both ϕ and $\dot{\varepsilon}_v$ of the samples decreased rapidly during the transient loading stage, while their decreasing trends were relatively steady during the creep stage. The main decrease in ϕ occurred during the transient loading stage. During the creep stage, the experimental conditions substantially influenced the $\dot{\varepsilon}_v$. For example, the $\dot{\varepsilon}_v$ of sample 45_04 with 0% moisture at 45 °C (Fig. 5c) was relatively low as compared to those of the other samples.

OAD Experimental Results and Analysis

The final porosity (ϕ_f) and the final volumetric strain rate ($\dot{\varepsilon}_{vf}$) of the salt sample were analyzed to indicate the effects of different factors on the compaction characteristics of the granular salt (Table 3). The corresponding conditions are listed in each row to provide an intuitive understanding of how the experimental conditions are related to each response. Both ϕ_f and $\dot{\varepsilon}_{vf}$ were used because these two parameters represent different physical meanings. The ϕ_f of the specimens indicates compression under the effects of the applied factors during the consolidation tests (including the transient loading stage and the creep stage), whereas the $\dot{\varepsilon}_{vf}$ represents the compression rate of the specimens in the creep stage. These two parameters can provide different guidance for practical engineering applications (ϕ_f for the optimal compression effect, and the

$\dot{\varepsilon}_{vf}$ for the optimal compression efficiency). These two parameters can provide different guidance for practical engineering applications. For example, the ϕ_f can be used to determine a more appropriate compression scheme when using granular salt for shaft sealing and mine backfilling with reference to the test results of ϕ . The $\dot{\varepsilon}_{vf}$ can be used to predict the long-term compression behavior of granular salt.

Direct Observation Analysis

The results of the OAD experiment can be treated statistically by direct observation analysis to evaluate the effect and importance of a given factor. In this analysis, the average response at each level for each factor was calculated from the data (Table 3) and the results are given in Tables 4 and 5. For example, the mean response of the first data point of temperature was the average of those obtained from experiments where the temperature was 30 °C (i.e., experiments 1, 2, 3, 4 and 5). Similarly, the mean response of the first data point of axial stress was the average of those obtained from experiments where the axial stress was 15 MPa (i.e., experiments 1, 6, 11, 16 and 21). The mean response of each level for a factor represented the degree of response of this level to the test results (ϕ or $\dot{\varepsilon}_v$ in our experiments), which were not affected statistically by the other factors in the experiment. Therefore, it was scientific and reliable to estimate the trend of the influence of a factor on the test results by the mean response of a factor at various levels. The effects of experimental factors on the mean responses for ϕ and $\dot{\varepsilon}_v$ are displayed in Figures 6 and 7, respectively.

According to Figs. 6a and 7a, the ϕ of the compacted salt samples was lower under higher ambient temperatures. As the ambient temperature increased, the $\dot{\varepsilon}_v$ of the compacted samples increased. Hence, it can be inferred that these two phenomena are unified in nature. Within the temperature range in our experiment (30–90 °C), the increase in ambient temperature accelerated the deformation of the granular salt samples, resulting in a faster deformation rate and a lower ϕ .

Figure 6b shows that the ϕ of the samples decreased with increasing compressive stress. Figure 7b presents a nonlinear relationship between the mean responses of the $\dot{\varepsilon}_v$ against the compressive stress. In general, a higher compressive stress corresponded to a lower ϕ , and the $\dot{\varepsilon}_v$ decreased as the

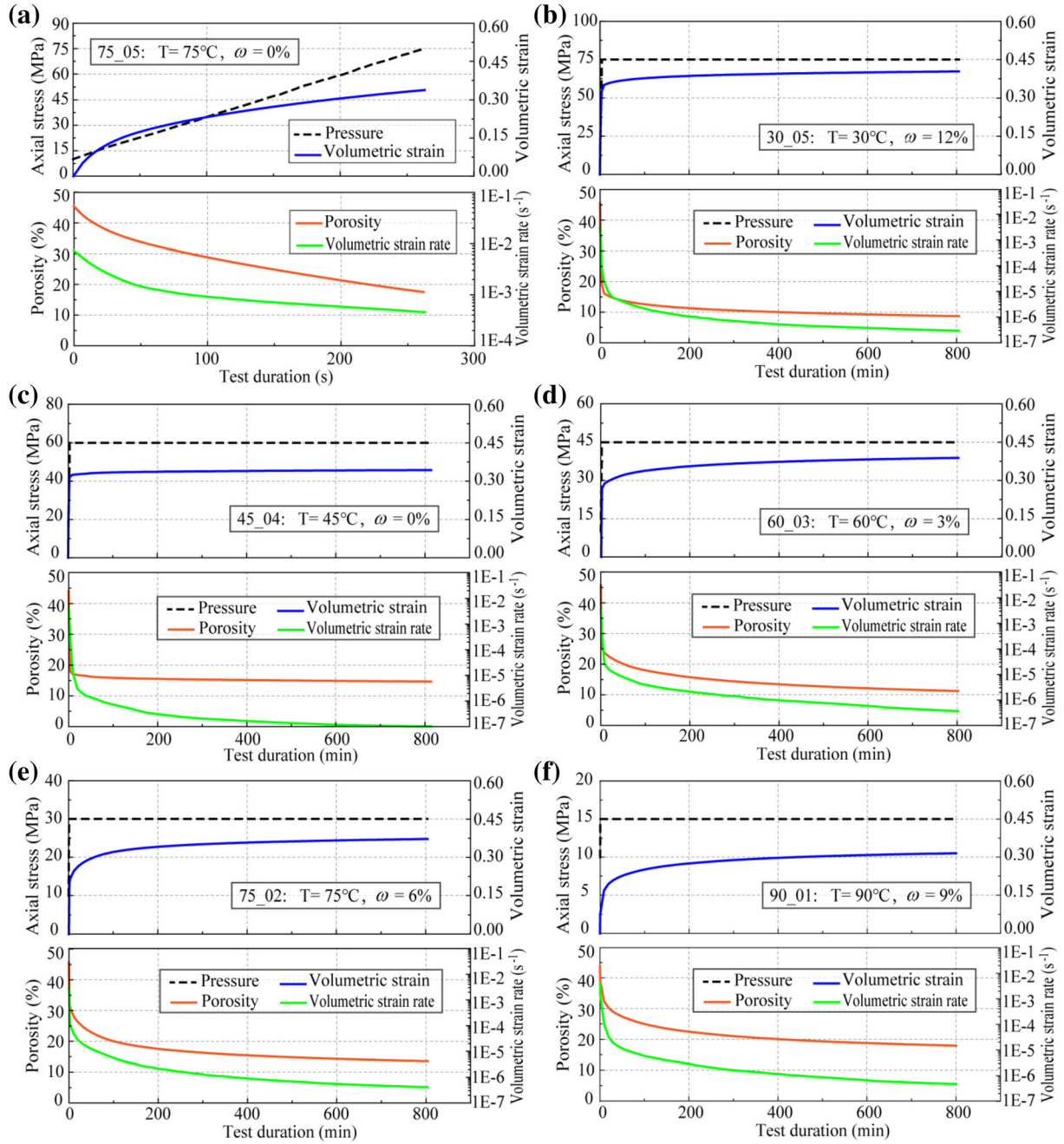


Fig. 5. Measured axial stress, volumetric strain, porosity and volumetric strain rate during the transient loading stage of sample (a) 75_05, and during the experiment for samples (b) 30_05, (c) 45_04, (d) 60_03, (e) 75_02 and (f) 90_01.

ϕ decreased (Fig. 5). In Figure 7b, the mean response for $\dot{\epsilon}_v$ also exhibited the above-mentioned trend when the axial stress was greater than 30 MPa. However, the trend was quite the opposite when the axial stress was 15 MPa. To clarify the mechanism

behind this phenomenon, the deformation characteristics of the granular samples during the transient loading stage were analyzed from another perspective. In Figure 8, the ϵ_v and $\dot{\epsilon}_v$ of sample 75_05 during the transient loading stage were plotted as a

Table 3. Experimental data and results

Exp. no.	Sample identification	Experimental factors				Responses		Permeability K (m ²)
		T (°C)	σ_1 (MPa)	ω (%)	T (min)	ϕ_f (%)	$\dot{\epsilon}_{vf}$ (s ⁻¹)	
1	30_01	30	15	0	50	33.69	5.15E-07	- ^a
2	30_02	30	30	3	100	18.55	4.00E-06	2.33E-14
3	30_03	30	45	6	200	13.70	1.15E-06	2.96E-15
4	30_04	30	60	9	400	9.20	4.66E-07	7.68E-17
5	30_05	30	75	12	800	8.69	2.94E-07	7.04E-17
6	45_01	45	15	6	100	22.31	5.32E-06	7.22E-14
7	45_02	45	30	9	200	16.64	3.08E-06	4.47E-15
8	45_03	45	45	12	400	11.34	9.30E-07	4.46E-16
9	45_04	45	60	0	800	14.68	1.03E-07	5.25E-15
10	45_05	45	75	3	50	10.91	4.02E-06	6.54E-16
11	60_01	60	15	12	200	19.65	3.07E-06	1.29E-14
12	60_02	60	30	0	400	19.85	1.02E-06	4.88E-14
13	60_03	60	45	3	800	11.25	3.64E-07	8.97E-16
14	60_04	60	60	6	50	12.18	8.05E-06	1.21E-16
15	60_05	60	75	9	100	8.83	3.42E-06	6.17E-17
16	75_01	75	15	3	400	21.26	1.77E-06	2.48E-14
17	75_02	75	30	6	800	13.53	4.08E-07	1.24E-15
18	75_03	75	45	9	50	14.91	9.96E-06	5.18E-16
19	75_04	75	60	12	100	9.17	3.31E-06	8.61E-17
20	75_05	75	75	0	200	10.44	2.03E-06	8.35E-17
21	90_01	90	15	9	800	17.92	4.72E-07	3.66E-15
22	90_02	90	30	12	50	18.16	1.11E-05	2.23E-15
23	90_03	90	45	0	100	14.07	4.72E-06	8.94E-16
24	90_04	90	60	3	200	9.65	1.76E-06	8.31E-17
25	90_05	90	75	6	400	6.73	4.36E-07	2.51E-17

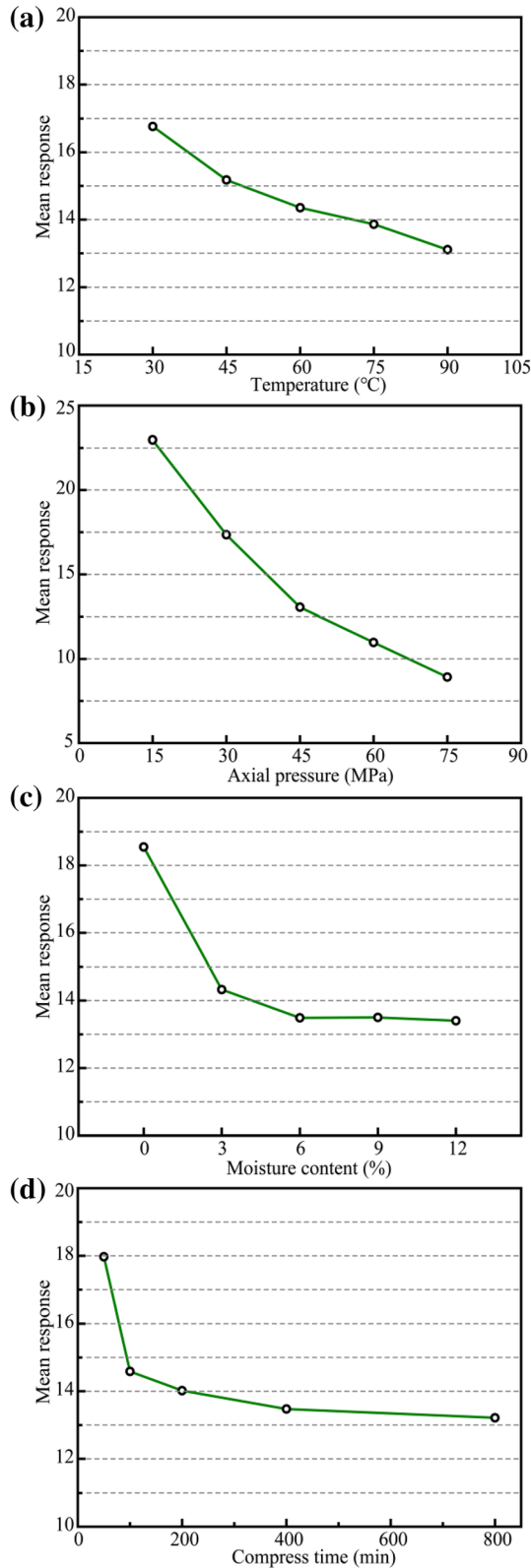
^aSample 30_01 was crushed while increasing the confining pressure in the permeability test because of its relatively low strength

Table 4. Mean response at each level of a factor and range of porosity (%)

Level	Experimental factors			
	Temperature (A)	Axial stress (B)	Moisture content (C)	Compression time (D)
1	16.766	22.966	18.546	17.970
2	15.176	17.346	14.324	14.586
3	14.352	13.054	13.490	14.016
4	13.862	10.976	13.500	13.476
5	13.106	8.920	13.402	13.214
Range (R)	3.660	14.046	5.144	4.756

Table 5. Mean response at each level of a factor and range of volumetric strain rate

Level	Experimental factors			
	Temperature (A)	Axial stress (B)	Moisture content (C)	Compression time (D)
1	1.28E-06	2.23E-06	1.68E-06	6.73E-06
2	2.69E-06	3.93E-06	2.38E-06	4.15E-06
3	3.18E-06	3.42E-06	3.12E-06	2.22E-06
4	3.50E-06	2.74E-06	3.48E-06	9.70E-07
5	3.74E-06	2.08E-06	3.74E-06	3.30E-07
Range (R)	2.46E-06	1.85E-06	2.06E-06	6.40E-06



◀ **Fig. 6.** Effect of controllable factors on the mean porosity responses.

function of the axial stress. The bilinear plots with two different slopes of the $\hat{\epsilon}_v$ data against the axial stress suggest that two compaction mechanisms (mechanisms 1 and 2) were present during the compaction of the granular salt. It may be inferred that mechanism 1 mainly involved the rearrangement of the granular salt, whereas mechanism 2 mainly involved the deformation of the granular salt caused by cataclastic flow of grains. The details of these mechanisms are described in section Microscopic Behavior of Consolidation.

According to Figs. 6c and 7c, the mean response for ϕ decreased with increasing moisture content. As the moisture content increased, the $\hat{\epsilon}_v$ of the samples under compaction increased. The variation in ϕ of the salt sample was slight when the moisture content was above 3%, whereas a stronger correlation was observed when the moisture content was less than 3% (Fig. 6c). According to Figure 6d, the mean response for ϕ decreased with increasing compression time, and the rate of decrease in ϕ decreased as the compression time increased. A similar trend was found in the mean responses of the strain rate as a function of compression time (Fig. 7d).

Range Analysis

The range analysis aimed to clarify the significance levels of influence of different factors on ϕ and $\hat{\epsilon}_v$ of the granular salt samples under compaction. The most significant factors can be determined based on the results of the range analysis. The larger the range value (R) is, the greater the significance level of factor impact is on an experimental index. The effect of each factor on a comprehensive evaluation index can be distinguished clearly even when the factors change. The R for each factor, which is the difference between the maximum and minimum values of the five levels, is given in Tables 4 and 5. The results for ϕ and $\hat{\epsilon}_v$ are shown in Figure 9 in the form of a histogram.

In Figure 9a, the sequence ($R_B > R_C > R_D > R_A$) showed the influence of the different factors on ϕ in descending order (where B is compressive stress, C moisture content, D compression time, A

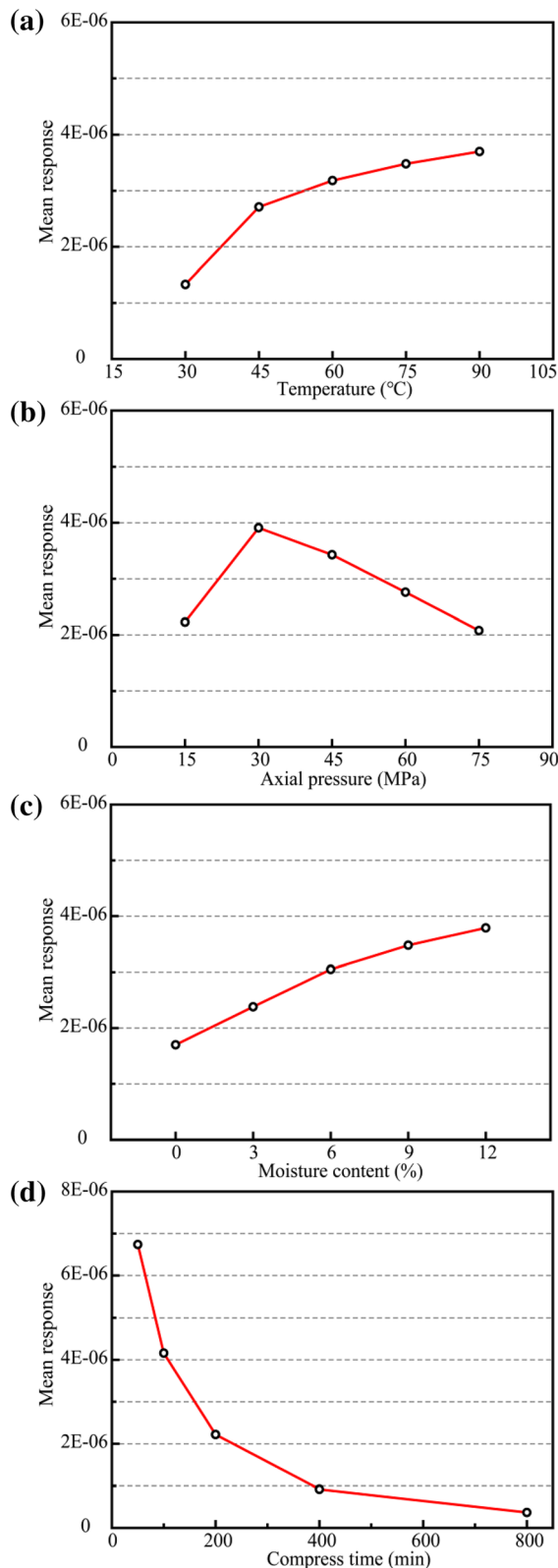
Fig. 7. Effect of controllable factors on the mean volumetric strain rate responses.

temperature). Hence, the axial stress had the greatest impact on ϕ of the granular salt sample, whereas temperature had the smallest impact on ϕ . Similarly in Figure 9b, the compression time had the greatest impact on $\dot{\epsilon}_v$, whereas temperature, moisture content and axial stress had smaller impacts on $\dot{\epsilon}_v$.

Analysis of Variance (ANOVA)

Variance reflects the volatility of the data, and it shows both the significance of the degree of change and the impact of factors on an index. To determine whether the difference between the results of the corresponding tests of each factor level was caused by the differences of levels or by the test error, an ANOVA of the test data was performed. In our experiments, two blank columns were set in the orthogonal array for error estimation so that it was unnecessary to repeat the experiments for each protocol. The sum of squares of deviation (SS), degree of freedom (DF) and mean squared deviation (MS) of ϕ and $\dot{\epsilon}_v$ were determined and are summarized in Tables 6 and 7. The F value of a factor was the ratio of the MS value of the factor to that of the error. By comparing the obtained F value with the theoretical one specific level and DF, the significance level can be determined for each factor.

The ANOVA results showed that the most important factor contributing to ϕ was axial stress, followed by moisture content, compression time and temperature. The compression time had the greatest impact on $\dot{\epsilon}_v$, whereas temperature, moisture content and axial stress had a smaller impact. The ANOVA results were consistent with the results of the range analysis. Additionally, the F test was performed for all the factors at 95% confidence level. Table 6 shows that the F value for all factors was greater than the critical F value ($F = 3.84$) from the standard table for 95% confidence level. This means that the variance of all factors was significant compared with the variance of the error and all factors had a meaningful effect on the responses. The comparison of the F value of each factor with the critical F value ($F = 3.84$) in Table 7 showed that the compression



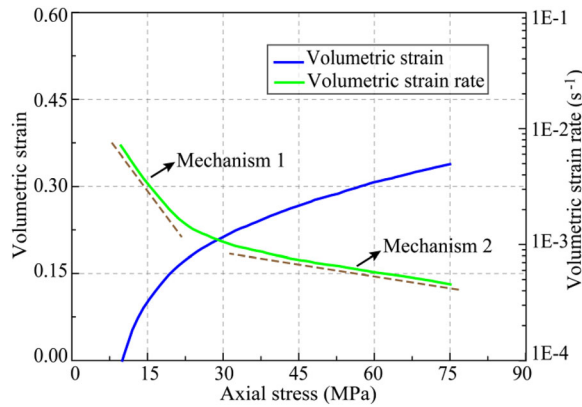


Fig. 8. Measured volumetric strain and volumetric strain rate versus axial stress during the transient loading stage of sample 75_05. The bilinear plots with two different slopes of the volumetric strain rate data against the axial stress suggest that two compaction mechanisms were present during the compaction of the granular salt.

time had a significant effect on $\dot{\epsilon}_v$. However, the F values for temperature, moisture content and axial stress were less than the critical F value ($F = 3.84$), indicating that the variance of temperature, moisture content and axial stress was nonsignificant compared to the variance of error. A comparison of the ANOVA results for the experimental responses of ϕ in Table 6 showed that this phenomenon may have been caused by exaggerated experimental errors resulting from possible interactions, which masked the significance of the factors.

Permeation Properties of Compacted Salt

After the compaction test was completed, the gas K of all the dried compacted salt samples was measured. Permeability measurements of the compacted salt samples were performed on a triaxial creep testing machine with axial flow geometry. The lowest value that this technique can measure was approximately 10^{-20} m^2 , which satisfied the accuracy requirement of our tests. Prior to the K measurements, all of the compacted salt samples were dried in a vacuum oven at 100°C for 48 h to avoid the water in the sample affecting the accuracy of the test. During each test, the compacted salt sample was compacted stepwise to a hydrostatic confining pressure of 5 MPa. Then, we adopted a steady-state flow method to measure the K of the compacted salt samples with nitrogen. Details of the K measurements can be found in our previous work (Liu et al.

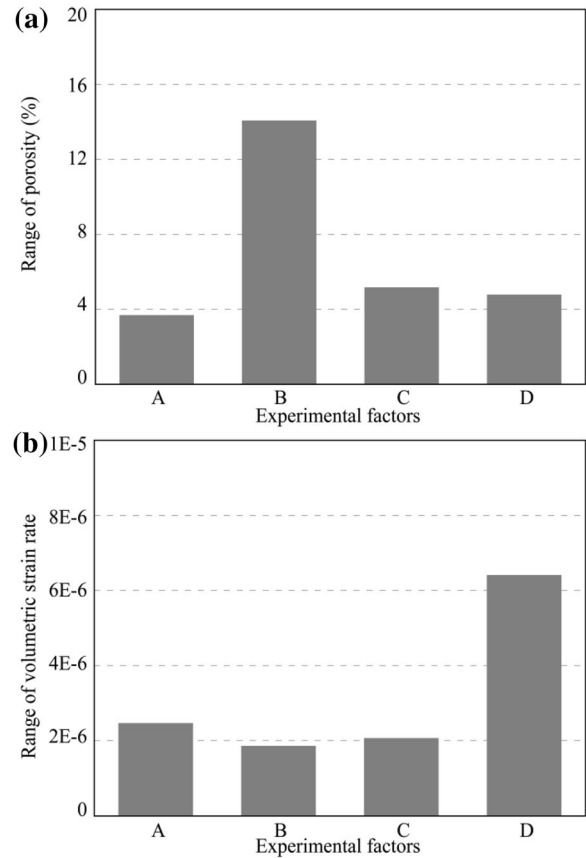


Fig. 9. Results of range analysis, where A is temperature, B compressive stress, C moisture content and D compression time.

2015, 2016). According to Darcy's law, the K (in m^2) of the samples can be derived as:

$$K = \frac{2P_0Q_0\mu L}{A(P_1^2 - P_2^2)} \quad (5)$$

where A is cross-sectional area (m^2) of a sample, L is sample length (m), Q_0 is volumetric flow rate (m^3/s) at atmospheric pressure, μ is dynamic viscosity (Pa s), P_0 is atmospheric pressure (Pa), P_1 is injection gas pressure (Pa), and P_2 is outlet gas pressure (Pa). During our measurement, the P_1 was kept at 1.0 MPa and the P_2 was approximately equal to the atmospheric pressure.

See Table 3 for the K of all dried compacted salt samples except for sample 30-01. The K of the compacted salt samples was as low as $2.51 \times 10^{-17} \text{ m}^2$. Achieving such a low K in such a short compression time indicated that compacted salt is very advantageous as a sealing material. Figure 10 shows the ϕ - K data derived from the mea-

Table 6. ANOVA results for experimental responses of porosity

Factors	SS	df	MS	F ^a	PC (%)	Significance
Temperature	39.24	4	9.81	5.31	4.64	*
Axial stress	626.51	4	156.63	84.84	74.14	*
Moisture content	97.55	4	24.39	13.21	11.45	*
Compress time	74.34	4	18.58	10.07	8.79	*
Error	14.77	8	1.85		0.88	

SS sum of squares, df degrees of freedom, MS mean squares, PC percentage contribution

^aCritical F value is 3.84 ($p < 0.05$)

Table 7. ANOVA results for experimental responses of volumetric strain rate

Factors	SS	df	MS	F ^a	PC (%)	Significance
Temperature	1.90E-11	4	4.75E-12	1.00	9.51	
Axial stress	1.23E-11	4	3.08E-12	0.64	6.17	
Moisture content	1.43E-11	4	3.58E-12	0.75	7.16	
Compress time	1.35E-10	4	3.38E-11	7.09	67.65	*
Error	3.80E-11	8	4.75E-12		9.51	

SS sum of squares, df degrees of freedom, MS mean squares, PC percentage contribution

^aCritical F value is 3.84 ($p < 0.05$)

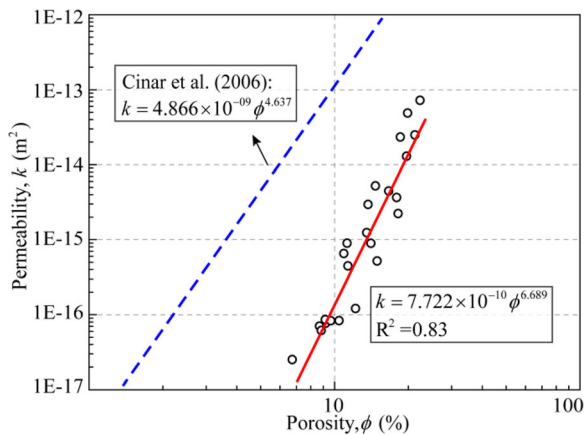


Fig. 10. Porosity–permeability correlation for the compacted salt samples.

measurements on the compacted salt samples. The correlation between ϕ and K of the compacted salt samples can be expressed as:

$$K = k_c \phi^n \tag{6}$$

where k_c and n are coefficients associated with the material. In our experiments, $k_c = 7.722 \times 10^{-10}$ and $n = 6.689$. This simple correlation between ϕ and K of the dried compacted salt samples (Fig. 10) was independent of the environmental and geological factors during the compaction of granular salt. It should be noted that such a simple correlation could

be meaningful for accurate predictions of the permeation properties of back-filled salt in the compaction process. A similar correlation between ϕ and K for compacted crushed NaCl granulates was reported by Cinar et al. (2006), which is also shown in Figure 10. The different coefficients (k_c and n) can be explained by the different salt materials and particle sizes. As shown in Figure 10, at the same ϕ , the compacted salt samples, which were compressed from fine-grained rock salt with a smaller particle size, had a lower K than the compacted salt samples in the literature (Cinar et al. 2006). This indicates that better sealing performance can be obtained by using compacted granular salt with a smaller initial particle size as a backfill material.

DISCUSSION

Non-negligible Deformation During Transient Loading

During the analysis of the orthogonal test results, the ϕ and $\dot{\epsilon}_v$ of the salt samples were selected to analyze the compaction characteristics of the granular salt. In previous studies, deformation during periods of transient loading (prior to creep) has often been neglected when characterizing viscous geologic materials such as salt (Lampe et al. 2018). However, the deformation curves (Fig. 5b–f) of the

granular salt samples showed that the deformation produced during the transient loading stage accounted for a considerable proportion of the total deformation. The ϕ change in random samples (samples 30_01 through 30_05) at different compression stages during compaction is shown in Figure 11. The figure shows that an appreciable amount of ϕ reduction occurred during the transient loading periods, which altered the ϕ_f to a considerable extent. As pressure increased, the proportion of ϕ reduction in the transient loading stage increased. In addition, the range analysis showed that the axial stress had the greatest impact on ϕ of the granular salt sample, whereas it had a comparatively less impact on $\dot{\epsilon}_v$, which implies that the effect of stress on the promotion of granular salt compaction mainly occurred in the transient loading stage. All these phenomena indicated that the deformation during the transient loading stage (i.e., prior to creep) needs to be considered thoroughly.

Microscopic Behavior of Consolidation

Granular salt consolidation is essentially a process of pore volume reduction, wherein the amount and nature of the final pore volume depend on multiple factors. Granular salt consolidation varies as a function of stress, temperature, moisture condition, time and impurity content (Mills et al. 2018). This section discusses the microscopic deformation behavior of pore reduction during granular salt compaction as well as how these factors affect this process. To reveal sample cohesiveness, grain boundary characteristics and other evidence of consolidation processes, the freshly broken aggregate

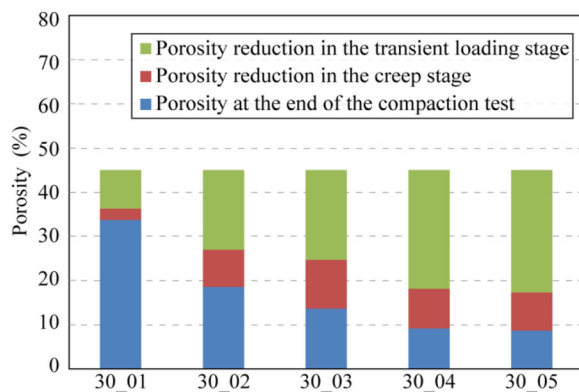


Fig. 11. Porosity change in the different compression stages.

surfaces of the compacted salt samples were observed microscopically using scanning electron microscope (SEM). The compacted salt samples were cut into sub-samples using a low-damage diamond wire, and fresh aggregate fragments were carefully broken from the sub-samples by hand to expose fresh surfaces. Then, the freshly broken aggregate surfaces were sprayed with a conductive coating in a vacuum chamber to improve the clarity and precision of the SEM images. A TESCAN VEGA 3 LMH was used to observe the freshly opened aggregate surface. SEM micrographs of the freshly broken aggregate surfaces are shown in Figure 12.

Deformation Mechanism During Compaction

For the deformation behavior during granular salt compaction, the total deformation, which is described by the strain tensor, is decomposed into time-independent and time-dependent deformation (Hansen et al. 2014). Time-independent deformation is related to elastic deformation and plastic deformation. Elastic deformation is generated during transient loading, whereas plastic deformation is induced by grain rearrangement, grain failure, grain sliding/rotation and the intra-grain sliding. Time-dependent deformation is mainly viscous deformation, which can be decomposed into viscous-elastic deformation and viscous-plastic deformation. The development of plastic deformation (including viscous-plastic deformation) of rock salt at temperatures in the range of 20–200 °C was summarized by Urai et al. (2008), as shown in Figure 13. Inter- and intra-granular micro-cracking, grain rotation and inter-granular slip are important strain accumulation processes alongside crystal plasticity (Fig. 13d) when subjected to low effective confining pressure and high deviatoric stresses (> 15–20 MPa). Dislocation creep (Fig. 13b), with the deformation mechanisms (Hansen 2014) of dislocation multiplication, glide, cross-slip and climb, are important, and rock salt can deform to large strains even at a low confining at temperatures in the range 100–200 °C. However, if the rock salt contains substantial amounts of water in the form of saturated brine inclusions or grain boundary films, dislocation creep can occur even at room temperature based on the process of fluid-assisted grain boundary migration which can reduce dislocation density and remove the stored energy of dislocations (Schenk and Urai 2004; Schenk et al.

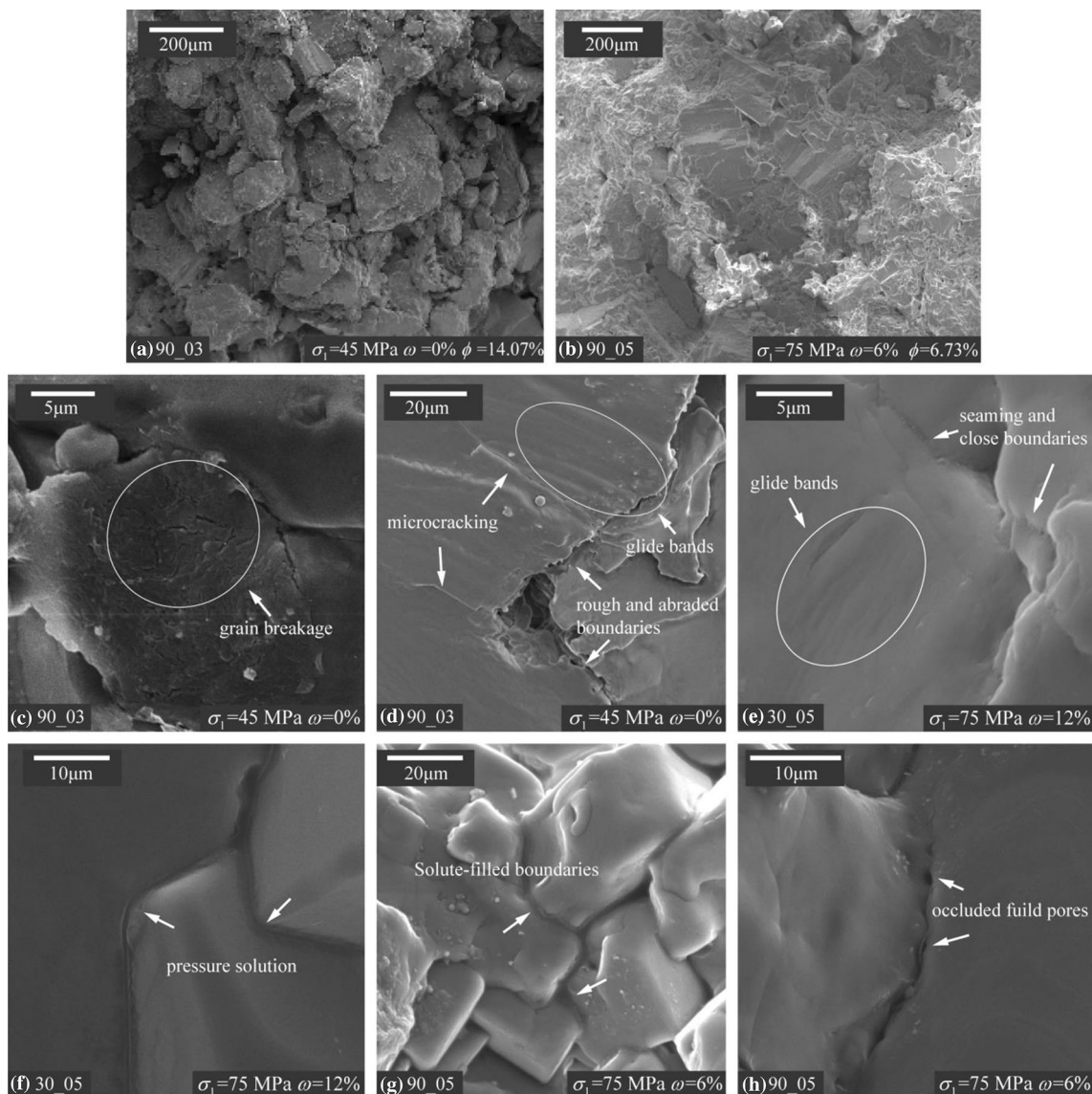


Fig. 12. SEM micrographs of freshly broken aggregates from the surfaces of different samples. (a) Sample 90_03: a compacted sample of granular salt without moisture, wherein the contact between grains was noncohesive. (b) Sample 90_05: a compacted sample of granular salt with 6% moisture content. (c) Sample 90_03: a sample containing grain breakage caused by extrusion. (d) Sample 90_03: a sample containing glide bands and micro-cracks due to grain sliding, grain boundaries lacking cohesion and rough, abraded surfaces. (e) Sample 30_05: a sample containing glide bands at inter-grain contacts and healed grain boundaries. (f) Sample 30_05: a sample containing pressure solution indents the grains; the arrows indicate indenting directions. (g) Sample 90_05: a sample containing pressure solution and grain boundaries filled with solute. (h) Sample 90_05: a sample containing healed grain boundaries and occluded fluid pores at the center along grain boundaries.

2006). Pressure-solution creep (Fig. 13c), also known as solution-precipitation creep, is a process whereby grains dissolve at highly stressed boundaries, solutes transport out of inter-granular contact sites through the grain boundary fluid, and the solutes precipitate on the less stressed faces of the

grains. This is another important deformation mechanism in most wet rock systems and is especially rapid in rock salt, which is accompanied by inter-granular sliding and rotation (grain re-arrangement), and can lead to compaction of porous salt or to deviatoric strain in nonporous aggregates

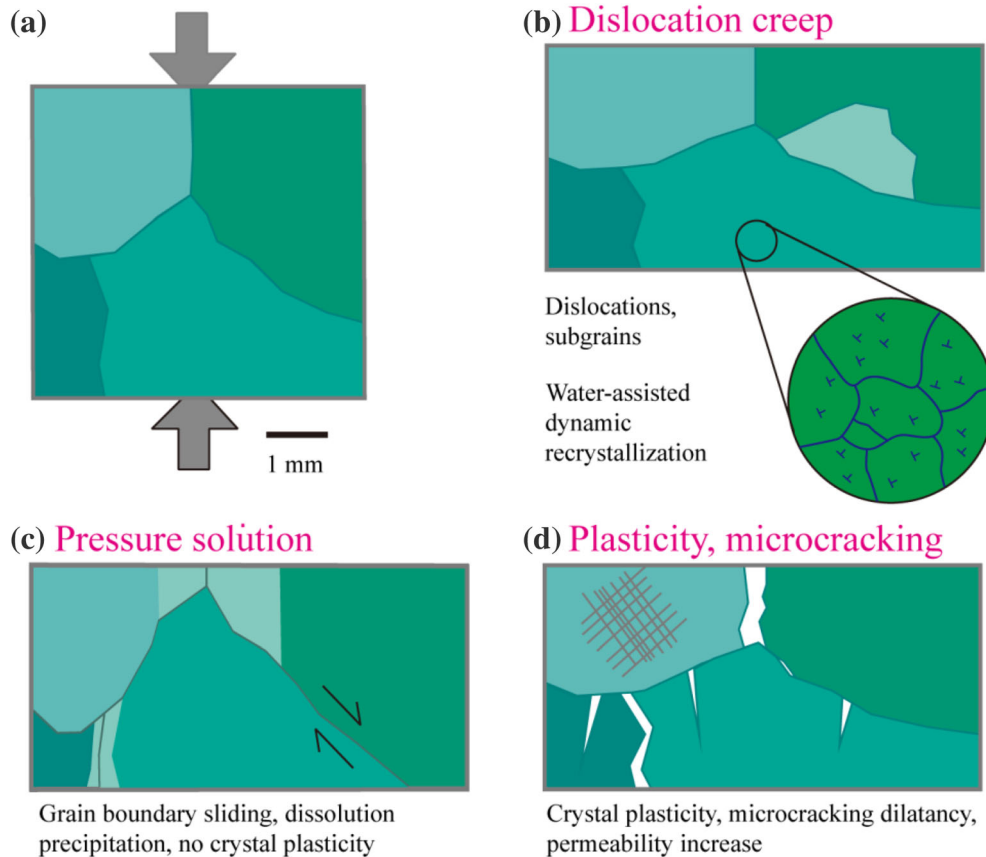


Fig. 13. Schematic drawing of micro-structural processes that can occur during deformation of halite at temperatures in the range of 20–200 °C (Urai et al. 2008). Different shades of green represent crystals with different orientations.

(Spiers and Schutjens 1999). The relative importance of the above process depends strongly on variables such as temperature, confining pressure, grain size and, importantly, on the presence of sufficient water in the grain boundaries to enable solution-precipitation phenomena. The fields in which different deformation mechanisms are dominant can be represented in deformation mechanism maps (Ter Heege et al. 2005a, b).

In our experiments, during the transient loading stage of granular salt compaction, the ϕ decreased rapidly (Fig. 5) under stress, creating a denser layer, which was accomplished by particle rearrangement and cataclastic flow. During the initial granular salt compaction, the applied stress induced particle rearrangement (mechanism 1 in Figure 8), including the translation and rotation of the particles. When the stress increased to the value that can cause damage to the granules (i.e., ~ 22 MPa in our experiments), cataclastic flow (mechanism 2 in Fig-

ure 8) occurred within the salt sample, which involved grain boundary slippage and particle breakage. During grain boundary sliding, the structure was deformed so heavily that dislocations were generated and grains slid and rubbed against each other (Fig. 12d and e). When the load reached the limit, thereby overcoming the ionic bonds in the rock salt, the grains fractured (Fig. 12c). In the constant-load creep stage of granular salt compaction, the stress did not continue to increase and additional ϕ reduction was dominated by crystal plasticity mechanisms and grain boundary processes. Dislocation creep (Fig. 13b), deformation, microcracking and crystal plasticity (Fig. 13d) occurred in dry granular salt. However, pressure solution (Fig. 13c) played a large role in the strain accumulation if some moisture was added to the granular salt. The traces of pressure solution (Fig. 12f and g) can be found throughout the SEM micrographs, indicating that pressure dissolution may be the main

mechanism for the compaction of wet granular salt. This was consistent with the flow laws in the deformation mechanism maps in the literature (Ter Heege et al. 2005a, b), wherein pressure-solution creep is strongly dependent on the grain size of the salt, and the fine-grained salt can increase the strain rate by more than two orders of magnitude.

In the process of granular salt compaction, nearly all deformation mechanisms are temperature dependent. Increase in temperature can enhance the velocity of dislocation motion (Ter Heege et al. 2005a), change the velocity and the characteristics of grain boundary migration (Piazolo et al. 2006), and accelerate the diffusion of solutes if water is present (Firme et al. 2016). As a result, the flow strength decreased and the compaction rate increased as temperature increased.

Promoting Effect of Water in Granular Salt Compaction

SEM micrographs of dry sample 90_3 are shown in Figure 12a, c and d. The broken and noncohesive grains in Figure 12a and the rough and abraded grain boundaries in Figure 12c and d provide evidence that grain boundary processes, such as pressure solution and recrystallization, cannot occur in the dry granular salt during compaction, which leads to a lower strain rate during compaction (Fig. 5c) and a higher ϕ (Fig. 6c). The ϕ of the sample with a moisture content of $\omega \geq 3\%$ was $\sim 30\%$ less than that of the sample with a moisture content of $\omega=0\%$. This reduction is a result of an additional fluid-assisted process, which plays a very important role during compaction. Moisture facilitates diffusion-controlled deformation mechanisms (i.e., pressure-solution creep and water-assisted dynamic recrystallization), again causing an associated reduction of 25–50% in the flow strength of the salt (Peach et al. 2001), thereby amplifying the compaction of crushed salt. The effects of moisture presented in Figure 12 are consistent with previous theories and studies on granular salt (Ter Heege et al. 2005a). However, a new contribution in this paper is that the limit of the amount of added moisture and its effectiveness during granular salt compaction can be determined based on variation in ϕ (Fig. 6c) from samples with various moisture contents.

Figure 14 shows the variation in water saturation during compaction of NaCl granulates as a

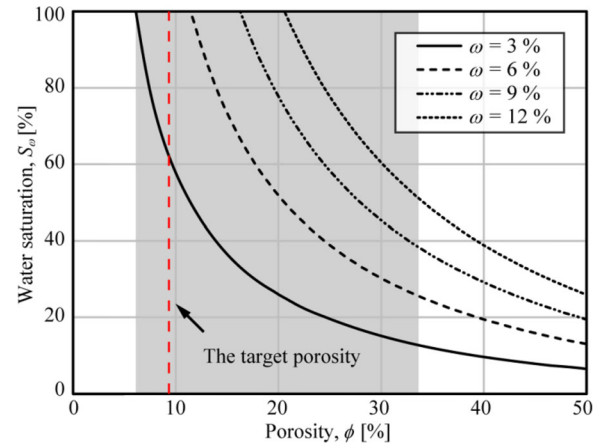


Fig. 14. Variation of water saturation (S_ω) in the granular salt during compaction as a function of porosity (ϕ) and initial moisture content (ω). The shaded part in the figure indicates the range of porosity of the samples obtained by the compaction experiments. The red dashed line indicates the target porosity, for which the corresponding permeability was $1 \times 10^{-16} \text{ m}^2$.

function of ϕ and moisture content, for which the constant water volume was assumed constant. The range of ϕ of the samples obtained from the compaction experiments is indicated by the shaded part in the figure. The water saturation (S_ω) can be calculated as:

$$S_\omega = \frac{V_w}{V_p} \quad (7)$$

where

$$V_w = \frac{m \cdot \omega}{\rho_w} \quad (8)$$

$$V_p = \frac{V_s \cdot \phi}{1 - \phi} \quad (9)$$

and

$$\rho_g = \frac{m}{V_s} \quad (10)$$

By combining Eqs. (7)–(10), the following formula can be obtained:

$$S_\omega = \frac{\rho_g \cdot \omega \cdot (1 - \phi)}{\rho_w \cdot \phi} \quad (11)$$

where V_w , V_p and V_s are volumes of water, pore space and salt grains in the sample, respectively, m is mass of a dry compacted salt specimen, ρ_w is water

density (taken as 1 g/cm^3), and ρ_g is salt grain density (taken as 2.16 g/cm^3).

As shown in Figure 14, the water saturation increased with decreasing ϕ , and the granular salt with higher initial moisture content more easily reached water saturation. According to Liu et al. (2016), the tightness of a salt cavern used for hydrocarbon energy storage can be guaranteed as long as the upper threshold K of the interlayers is not more than 10^{-16} m^2 . Therefore, the target ϕ of the compaction of granular salt can be defined as the corresponding ϕ when the K is 10^{-16} m^2 , which can be calculated by Eq. 6. The target ϕ was marked with a red dashed line in Figure 14. In the case of no drainage (i.e., water volume is constant during compaction), high water saturations in pore space during compaction reduce the volume of compressible air, which leads to increases in pore pressure and decreases in effective compaction stresses. Therefore, based on water saturation reaching 60% at the target ϕ when the initial water content was 3%, it was suggested that the initial moisture content of the granular salt should not exceed 3% in the case of no drainage.

For the compaction experiments in this paper, the samples were drained during compaction so that the effective compaction stress would not be affected even if the initial moisture content increased. In this case, the increase in water saturation promoted water-assisted grain boundary processes, such as pressure solution and recrystallization. However, Figure 14 shows that the water can reach saturation state before the ϕ reached the target ϕ even if the initial water cut was only 6%. This may explain why the ϕ did not continue to decrease (Fig. 6c) when the initial water content exceeded 6%. Therefore, it was suggested that the initial moisture content of the granular salt should be in the range of 3–6% in the case of drainage.

Long-Term Permeability Evolution

Grain boundary healing was found in the SEM micrographs of samples 30_5 (Fig. 12e) and 90_5 (Fig. 12g and h), which suggests that the self-healing properties of rock salt cannot be ignored when evaluating the long-term K of compacted salt. The self-healing properties of rock salt have been studied

by many scholars (Arson et al. 2012; Desbois et al. 2012; Chen et al. 2013; Arson 2020), and the physical mechanisms were summarized by Houben et al. (2013), as shown in Figure 15. First, there is purely mechanical closure of cracks due to compaction of the bulk rock by elastic deformation, plastic flow or flow by pressure solution, occurring in a regime of increasing mean normal stress (Fig. 15a) (Chan et al. 2000). The second mechanism is diffusion or “chemical” crack healing driven by surface energy reduction (Fig. 15b) (Urai et al. 1986; Schenk et al. 2006). This mechanism involves the necking down of cracks to form tubes and eventually isolated, sub-spherical fluid inclusions. In this case, transport of material occurs by diffusion through thin water films adsorbed to the solid surface or completely filling the cracks. The last mechanism, crack healing by recrystallization, is a process in which grain boundary migration of fluid-filled grain boundaries overgrows the crack, leaving sub-spherical fluid inclusions behind (Fig. 15c) (Ter Heege et al. 2005b; Urai and Spiers 2007). The healing process with all mechanisms can substantially reduce the K of the compaction by changing the size and connectivity of the pores and cracks (Chan et al. 2001). Diffusion healing and recrystallization healing are expected to play an important role in the long-term evolution of K .

A microscopic/macrosopic healing model based on pressure solution (Shen and Arson 2019a, b) and diffusion (Zhu and Arson 2015a, b) was established and calibrated against granular salt creep tests in the laboratory. The numerical simulation results when using the model showed that the healing rate was very sensitive to crystal size and can increase substantially with smaller crystal size; the healing rate increased substantially when the component of compressive stress normal to the grain-to-grain contact plane increased. For uniform void size distributions, the healing rate initially increased, but the ϕ_f change did not depend on the initial ϕ ; crack healing can occur within a few days at room temperature and low pressure and it can be enhanced at higher temperatures. These conclusions can provide a reference for predicting the long-term evolution of K . However, the establishment of mathematical relationships to describe the effect of healing on the long-term K of compacted salt requires more experimentation.

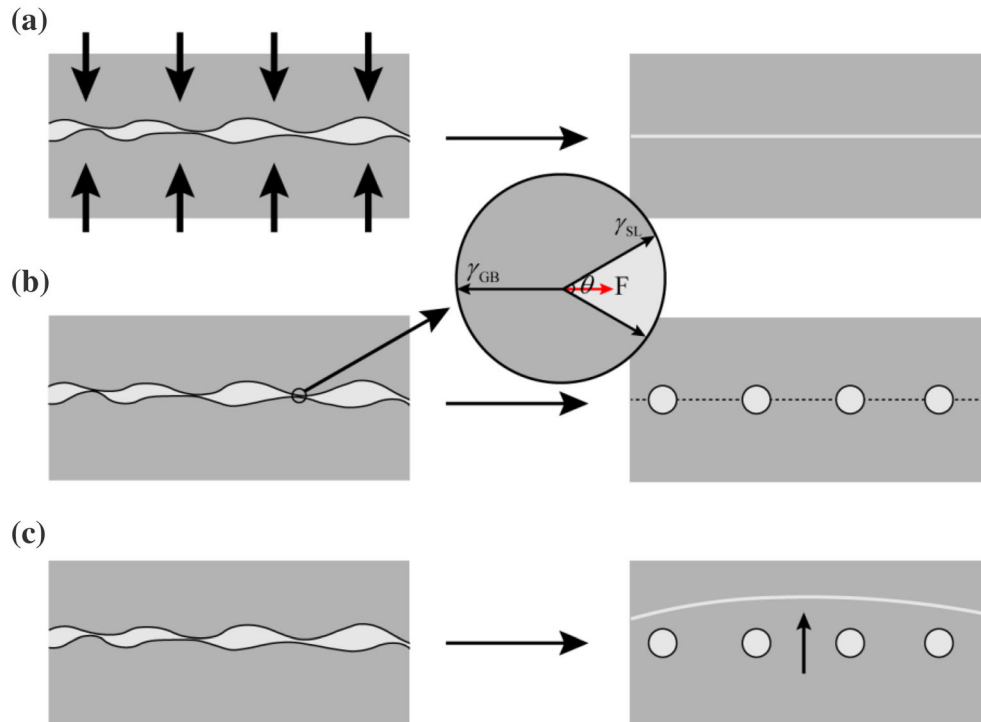


Fig. 15. Physical mechanisms by which crack healing/sealing and permeability reduction can occur in rock salt (Houben et al. 2013). (a) Mechanical closure of cracks in association with compaction of bulk rock by elastic deformation or plastic flow. (b) Necking (occlusion) cracks and pores to form arrays of disconnected tubular and spherical inclusions, by means of surface energy-driven, diffusive mass transport facilitated by adsorbed water films or free pore brine. (c) Crack and pore occlusion through fluid-assisted grain boundary migration (recrystallization).

Implications for Engineering Applications

Some implications that can be referred to when using granular salt for shaft sealing and mine backfilling are summarized as follows, based on the results of the OAD experiments and the microscopic behavior of consolidation:

- (1) The ϕ of compacted salt was largely controlled by compressive stress, and the main deformation occurred during the transient loading phase.
- (2) Adding moisture to granular salt can facilitate compaction greatly, but a limit exists for the amount of added moisture and for its effectiveness. It was suggested that the initial moisture content of the granular salt should not exceed 3% in the case of no drainage, whereas it should be 3–6% in the case of drainage.
- (3) The strain rate in the creep stage was affected mainly by compression time,

whereas the compressive stress played a very slight role. Pressure solution and water-assisted recrystallization may be the main deformation mechanism during the creep stage if sufficient water exists in the grain boundaries.

- (4) Increasing the temperature was beneficial to the compaction of granular salt, which can increase the strain rate and healing rate during compaction.
- (5) Fine granular salt was recommended to be compacted for use in shaft sealing and mine backfilling based on the high sensitivity of the pressure solution and healing to the grain size of the salt.
- (6) The decrease in K of the compacted salt depended mainly on the decrease in ϕ , but the long-term K evolution may be affected by the self-healing properties of the material, which is conducive to safe long-term sealing.

CONCLUSIONS

An orthogonal array design experimental plan and a series of compression experiments were performed to evaluate the influence of environmental factors on the reconsolidation behavior of fine granular salt. Accordingly, an $L_{25} (5^6)$ matrix was chosen to evaluate the effects of the proposed factors (temperature, compressive stress, moisture content and compression time) on the responses of porosity and the volumetric strain rate. The results showed that these proposed factors had significant impacts on the granular salt compaction properties. In this research, we investigated the comprehensive effect of various geological and environmental factors, the threshold of moisture content effect on salt grain compaction and the relative weights of various factors on the compression effect.

- (1) Compressive stress had the greatest impact on porosity of the granular salt sample, and the porosity of the samples decreased with increasing compressive stress. However, during the creep stage, the effect of compressive stress on volumetric strain rate was relatively small. Adding moisture to the granular salt can greatly reduce the porosity of the sample, whereas the effect was limited when moisture exceeded 3%. In the process of granular salt compaction, nearly all deformation mechanisms were temperature dependent.
- (2) An increase in temperature can accelerate the volumetric strain rate resulting in decrease in porosity. The volumetric strain rate reduction during the creep stage was mainly determined by compression time and was affected by factors such as temperature and moisture content. In addition, the results showed that the deformation during the transient loading process cannot be ignored when attempting to predict transient material behavior accurately.
- (3) The correlation between porosity and permeability of the dried compacted salt samples was independent of the environmental and geological factors during the compaction of granular salt. Moreover, a better sealing performance can be obtained by using compacted granular salt with a smaller initial particle size as a backfill material.

- (4) In the transient loading stage of granular salt compaction, the porosity decreased rapidly under stress, thereby forming a denser layer, which was accomplished by particle rearrangement and cataclastic flow. In the constant-load creep stage of granular salt compaction, the stress did not continue to increase, and the additional porosity reduction was dominated by grain boundary processes and crystal plasticity mechanisms, including dislocation creep, pressure-solution creep and recrystallization. Pressure solution and recrystallization may be the main deformation mechanism during the creep stage in the presence of sufficient water around the grain boundaries.

ACKNOWLEDGMENTS

This work was supported by the National Natural Science Foundation of China (Nos. 51834003, 41672292, 51904039, 41702309) and Chongqing Postdoctoral Science Foundation (cstc2019jcyj-bshX0084), which are all greatly appreciated.

REFERENCES

- Arson, C. (2020). Micro-macro mechanics of damage and healing in rocks. *Open Geomechanics*, 2, 1–41.
- Arson, C., Xu, H., & Chester, F. M. (2012). On the definition of damage in time-dependent healing models for salt rock. *Géotechnique Letters*, 2(2), 67–71.
- Bauer, S., & Urquhart, A. (2016). Thermal and physical properties of reconsolidated crushed rock salt as a function of porosity and temperature. *Acta Geotechnica*, 11(4), 913–924.
- Bechthold, W., Smailos, E., Heusermann, S., Bollingerfehr, W., Bazargan Sabet, B., Rothfuchs, T., et al. (2004). Backfilling and sealing of underground repositories for radioactive waste in salt (BAMBUS-II Project). *Final report for European atomic energy community EUR 20621*. Luxembourg: Office for Official Publications of the European Communities.
- Broome, S., Bauer, S., & Hansen, F. (2014). Reconsolidation of crushed salt to 250°C under hydrostatic and shear stress conditions. In *48th US rock mechanics/geomechanics symposium*, June 1–4, 2014, Minneapolis, Minnesota.
- Chan, K. S., Bodner, S. R., & Munson, D. E. (2001). Permeability of WIPP salt during damage evolution and healing. *International Journal of Damage Mechanics*, 10(3), 347–375.
- Chan, K. S., Bodner, S. R., Munson, D. E., & Munson, D. E. (2000). Application of isochronous healing curves in predicting damage evolution in a salt structure. *International Journal of Damage Mechanics*, 9(2), 130–153.

- Chen, J., Kang, Y., Liu, W., Fan, J., Jiang, D., & Chemenda, A. (2018). Self-healing capacity of damaged rock salt with different initial damage. *Geomechanics and Engineering*, 15(1), 615–620.
- Chen, J., Liu, W., Jiang, D., Zhang, J., Ren, S., Li, L., et al. (2017). Preliminary investigation on the feasibility of a clean CAES system coupled with wind and solar energy in China. *Energy*, 127, 462–478.
- Chen, J., Lu, D., Liu, W., Fan, J., Jiang, D., Yi, L., et al. (2020). Stability study and optimization design of small-spacing two-well (SSTW) salt caverns for natural gas storages. *Journal of Energy Storage*. <https://doi.org/10.1016/j.est.2019.101131>.
- Chen, J., Ren, S., Yang, C., Jiang, D., & Li, L. (2013). Self-healing characteristics of damaged rock salt under different healing conditions. *Materials*, 6(8), 3438–3450.
- Cinar, Y., Pusch, G., & Reitenbach, V. (2006). Petrophysical and capillary properties of compacted salt. *Transport in Porous Media*, 64(2), 199–228.
- Costa, A., Amaral, C., & Poiate, E., Jr. (2015). Hydrocarbon production and storage using offshore underground salt caverns. In L. Roberts, K. Mellegard, & F. Hansen (Eds.), *Mechanical behaviour of salt VIII* (pp. 209–216). London: Taylor & Francis Group.
- Creti, A. (2009). *The economics of natural gas storage: A European perspective*. Berlin: Springer.
- Desbois, G., Urai, J. L., Schmatz, J., Zavada, P., & de Bresser, H. (2012). The distribution of fluids in natural rock salt to understand deformation mechanisms. In P. Berest, M. Ghoreychi, F. Hadj-Hassen, & M. Tijani (Eds.), *Mechanical behavior of salt VII* (pp. 3–12). London: Taylor & Francis Group.
- Dewers, T., Heath, J. E., & Leigh, C. D. (2015). Transport properties of run-of-mine salt backfill? Unconsolidated to consolidated. In No. SAND2015-8677R. Albuquerque, NM: Sandia National Lab.
- Ding, J., Chester, F. M., Chester, J. S., Zhu, C., & Arson, C. (2016). Mechanical behavior and microstructure development in consolidation of nominally dry granular salt. In *50th US rock mechanics/geomechanics symposium*, June 26–29, 2016, Houston, Texas.
- Fan, J., Jiang, D., Chen, J., Liu, W., Ngaha, W. T., & Chen, J. (2018). Fatigue performance of ordinary concrete under discontinuous cyclic loading. *Construction and Building Materials*, 166, 974–981.
- Fan, J., Jiang, D., Liu, W., Wu, F., Chen, J., & Daemen, J. (2019). Discontinuous fatigue of salt rock with low-stress intervals. *International Journal of Rock Mechanics and Mining Sciences*, 115, 77–86.
- Fan, J., Liu, W., Jiang, D., Chen, J., Tiedeu, W. N., & Daemen, J. J. (2020a). Time interval effect in triaxial discontinuous cyclic compression tests and simulations for the residual stress in rock salt. *Rock Mech Rock Eng*. <https://doi.org/10.1007/s00603-020-02150-y>.
- Fan, J., Liu, P., & Li, J. (2020b). A coupled methane/air flow model for coal gas drainage: model development and finite-difference solution. *Process Safety and Environmental Protection*, 141(8), 288–304.
- Firme, P. A., Roehl, D., & Romanel, C. (2016). An assessment of the creep behaviour of Brazilian salt rocks using the multi-mechanism deformation model. *Acta Geotechnica*, 11(6), 1445–1463.
- Hansen, F. D. (2014). Micromechanics of isochoric salt deformation. In *48th US rock mechanics/geomechanics symposium*, June 1–4, 2014, Minneapolis, Minnesota.
- Hansen, F. D., Bauer, S., Broome, S., & Callahan, G. (2012). Coupled thermal-hydrological-mechanical processes in salt: Hot granular salt consolidation, constitutive model and micromechanics. In No. SAND2012-9893P. Albuquerque, NM: Sandia National Laboratories.
- Hansen, F. D., & Leigh, C. D. (2011). Salt disposal of heat-generating nuclear waste. In No. SAND2011-0161. Albuquerque, NM: Sandia National Laboratories.
- Hansen, F. D., Popp, T., Wieczorek, K., & Stuehrenberg, D. (2014). Granular salt summary: Salt reconsolidation principles and application. In No. SAND2014-16141R. Albuquerque, NM: Sandia National Laboratories.
- Hart, D. (2018). An analysis of possible salt fall events in historical pressure data from the US strategic petroleum reserve. In No. SAND-2018-11419. Albuquerque, NM: Sandia National Lab.
- Houben, M. E., ten Hove, A., Peach, C. J., & Spiers, C. J. (2013). Crack healing in rocksalt via diffusion in adsorbed aqueous films: microphysical modelling versus experiments. *Physics and Chemistry of the Earth, Parts A/B/C*, 64, 95–104.
- Jiang, D., Fan, J., Chen, J., Li, L., & Cui, Y. (2016). A mechanism of fatigue in salt under discontinuous cycle loading. *International Journal of Rock Mechanics and Mining Sciences*, 100(86), 255–260.
- Kang, Y., Chen, J., Jiang, D., Liu, W., & Fan, J. (2019). Summary on damage self-healing property of rock salt. *Rock and Soil Mechanics*, 40(1), 55–69.
- Khamrat, S., & Fuenkajorn, K. (2018). Mechanical performance of consolidated crushed salt as backfill in boreholes and shafts. *Songklanakarin Journal of Science and Technology*, 40(2), 431–439.
- Khamrat, S., Tepnarong, P., Artkhonghan, K., & Fuenkajorn, K. (2018). Crushed salt consolidation for borehole sealing in potash mines. *Geotechnical and Geological Engineering*, 36(1), 49–62.
- Lampe, B. C., Stormont, J. C., Lynn, T. D., & Bauer, S. J. (2018). Experimental investigation of the influence of pore pressure and porosity on the deformation of granular salt. *International Journal of Rock Mechanics and Mining Sciences*, 110, 291–305.
- Letcher, T. M. (2019). Storing electrical energy. In T. M. Letcher (Ed.), *Managing global warming: An interface of technology and human issues* (pp. 365–377). Amsterdam: Elsevier.
- Li, J., Shi, X., & Zhang, S. (2020). Construction modeling and parameter optimization of multi-step horizontal energy storage salt caverns. *Energy*. <https://doi.org/10.1016/j.energy.2020.117840>.
- Liu, W., Chen, J., Jiang, D., Shi, X., Li, Y., Daemen, J. J. K., et al. (2016). Tightness and suitability evaluation of abandoned salt caverns served as hydrocarbon energies storage under adverse geological conditions (AGC). *Applied Energy*, 178, 703–720.
- Liu, E., Li, W., Cai, H., & Peng, S. (2019a). Formation mechanism of trailing oil in product oil pipeline. *Processes*, 7(1), 7.
- Liu, W., Li, Y., Yang, C., Daemen, J. J., Yang, Y., & Zhang, G. (2015). Permeability characteristics of mudstone cap rock and interlayers in bedded salt formations and tightness assessment for underground gas storage caverns. *Engineering Geology*, 193, 212–223.
- Liu, E., Lv, L., Yi, Y., & Xie, P. (2019b). Research on the steady operation optimization model of natural gas pipeline considering the combined operation of air coolers and compressors. *IEEE Access*, 7, 83251–83265.
- Liu, W., Zhang, Z., Chen, J., Fan, J., Jiang, D., Jjk, D., et al. (2019c). Physical simulation of construction and control of two butted-well horizontal cavern energy storage using large molded rock salt specimens. *Energy*, 185, 682–694.
- Liu, W., Zhang, X., Fan, J., Li, Y., & Wang, L. (2020). Evaluation of potential for salt cavern gas storage and integration of brine extraction: Cavern utilization, Yangtze River Delta region. *Natural Resources Research*. <https://doi.org/10.1007/s11053-020-09640-4>.

- Mills, M. M., Stormont, J. C., & Bauer, S. J. (2018). Micromechanical processes in consolidated granular salt. *Engineering Geology*, 239, 206–213.
- Olivella, S., Castagna, S., Alonso, E., & Lloret, A. (2011). Porosity variations in saline media induced by temperature gradients: Experimental evidences and modelling. *Transport in Porous Media*, 90(3), 763–777.
- Paneru, L. P., Bauer, S. J., & Stormont, J. C. (2018). Thermal properties of consolidated granular salt as a backfill material. *Rock Mechanics and Rock Engineering*, 51(3), 911–923.
- Peach, C. J., Spiers, C. J., & Trimby, P. W. (2001). Effect of confining pressure on dilatation, recrystallization and flow of rocksalt at 150°C. *Journal of Geophysical Research Solid Earth*, 106(B7), 13315–13328.
- Peng, H., Fan, J., Zhang, X., Chen, J., Li, Z., Jiang, D., et al. (2020). Computed tomography analysis on cyclic fatigue and damage properties of rock salt under gas pressure. *International Journal of Fatigue*. <https://doi.org/10.1016/j.ijfatigue.2020.105523>.
- Piazolo, S., Bestmann, M., Prior, D., & Spiers, C. (2006). Temperature dependent grain boundary migration in deformed-then-annealed material: Observations from experimentally deformed synthetic rocksalt. *Tectonophysics*, 427(1–4), 55–71.
- Popp, T., Minkley, W., Salzer, K., & Schulze, O. (2012). Gas transport properties of rock salt—synoptic view. In P. Berest, M. Ghoreychi, F. Hadj-Hassen, & M. Tijani (Eds.), *Mechanical behavior of salt VII* (pp. 143–153). London: Taylor & Francis Group.
- Qiao, W., Yang, Z., Kang, Z., & Pan, Z. (2020). Short-term natural gas consumption prediction based on Volterra adaptive filter and improved whale optimization algorithm. *Engineering Applications of Artificial Intelligence*. <https://doi.org/10.1016/j.engappai.2019.103323>.
- Salzer, K., Popp, T., & Böhnelt, H. (2007). Mechanical and permeability properties of highly pre-compacted granular salt bricks. In K.-H. Lux, W. Minkley, M. Wallner, & H. R. Hardy Jr. (Eds.), *Basic and applied salt mechanics: Proceedings of the 6th conference on the mechanical behavior of salt* (pp. 239–248). Hannover: Francis & Taylor.
- Schenk, O., & Urai, J. L. (2004). Microstructural evolution and grain boundary structure during static recrystallization in synthetic polycrystals of sodium chloride containing saturated brine. *Contributions to Mineralogy and Petrology*, 146(6), 671–682.
- Schenk, O., Urai, J. L., & Piazolo, S. (2006). Structure of grain boundaries in wet, synthetic polycrystalline, statically recrystallizing halite—evidence from cryo-SEM observations. *Geofluids*, 6(1), 93–104.
- Schiebahn, S., Grube, T., Robinius, M., Tietze, V., Kumar, B., & Stolten, D. (2015). Power to gas: Technological overview, systems analysis and economic assessment for a case study in Germany. *International Journal of Hydrogen Energy*, 40(12), 4285–4294.
- Shen, X., & Arson, C. (2019a). An isotropic self-consistent homogenization scheme for chemo-mechanical healing driven by pressure solution in halite. *International Journal of Solids and Structures*, 161, 96–110.
- Shen, X., & Arson, C. (2019b). Simulation of salt-cavity healing based on a micro–macro model of pressure solution. *Petroleum Geoscience*, 25(3), 251–257.
- Shi, X., Li, Y., Yang, C., Xu, Y., Ma, H., Liu, W., et al. (2015). Influences of filling abandoned salt caverns with alkali wastes on surface subsidence. *Environmental Earth Sciences*, 73(11), 6939–6950.
- Spiers, C. J., & Schutjens, P. M. T. M. (1999). Intergranular pressure solution in NaCl: Grain-to-grain contact experiments under the optical microscope dissolution sous contrainte dans NaCl: Expériences de contact grain à grain sous microscope optique. *Oil & Gas Science & Technology*, 54(6), 729–750.
- Tarkowski, R., & Czapowski, G. (2018). Salt domes in Poland—potential sites for hydrogen storage in caverns. *International Journal of Hydrogen Energy*, 43(46), 21414–21427.
- Ter Heege, J. H., De Bresser, J., & Spiers, C. (2005a). Rheological behaviour of synthetic rocksalt: the interplay between water, dynamic recrystallization and deformation mechanisms. *Journal of Structural Geology*, 27(6), 948–963.
- Ter Heege, J. H., De Bresser, J. H. P., & Spiers, C. J. (2005b). Dynamic recrystallization of wet synthetic polycrystalline halite: dependence of grain size distribution on flow stress, temperature and strain. *Tectonophysics*, 396(1–2), 35–57.
- Urai, J. L., Schléder, Z., Spiers, C., & Kukla, P. (2008). Flow and transport properties of salt rocks. In R. Littke, U. Bayer, D. Gajewski, & S. Nelskamp (Eds.), *Dynamics of complex intracontinental basins: the central European basin system* (pp. 277–290). Berlin: Springer.
- Urai, J. L., & Spiers, C. (2007). The effect of grain boundary water on deformation mechanisms and rheology of rocksalt during long-term deformation. In M. Wallner, K.-H. Lux, W. Minkley, & H. Hardy (Eds.), *The mechanical behaviour of salt—understanding of THMC processes in salt* (pp. 149–158). London: Taylor & Francis.
- Urai, J. L., Spiers, C., Zwart, H. J., & Lister, G. S. (1986). Weakening of rock salt by water during long-term creep. *Nature*, 324(6097), 554–557.
- Wang, J., Zhang, Q., Song, Z., & Zhang, Y. (2020). Creep properties and damage constitutive model of salt rock under uniaxial compression. *International Journal of Damage Mechanics*, 29(6), 902–922.
- Wu, F., Gao, R., Liu, J., & Li, C. (2020). New fractional variable-order creep model with short memory. *Applied Mathematics and Computation*. <https://doi.org/10.1016/j.amc.2020.125278>.
- Zhang, N., Shi, X., Zhang, Y., & Shan, P. (2020). Tightness analysis of underground natural gas and oil storage caverns with limit pillar widths in bedded rock salt. *IEEE Access*, 8, 12130–12145.
- Zhu, C., & Arson, C. (2015a). Fabric-enriched modeling of anisotropic healing induced by diffusion in granular salt. In *The 49th US rock mechanics/geomechanics symposium*, 28 June–1 July 2015, San Francisco, CA.
- Zhu, C., & Arson, C. (2015b). A model of damage and healing coupling halite thermo-mechanical behavior to microstructure evolution. *Geotechnical and Geological Engineering*, 33(2), 389–410.